Brillouin-scattering studies of ferroelectric $[NH_3(CH_3)]_5Bi_2Cl_{11}$

B. Mróz
Institute of Physics, A. Mickiewicz University, Umultowska 85, 61-614 Poznań, Poland

J. A. Tuszyński
Department of Physics, University of Alberta, Edmonton, Alberta, Canada T6G 2J1

H. Kiefte and M. J. Clouter
Department of Physics and Physical Oceanography, Memorial University of Newfoundland, St. John's, Newfoundland, Canada A1B 3X7

R. Jakubas
Faculty of Chemistry, Wroclaw University, Joliot-Curie 14, 50-383 Wroclaw, Poland

D. Sept
Department of Chemistry and Biochemistry, University of California, San Diego, La Jolla, California 92093-0305

(Received 14 August 1997; revised manuscript received 18 March 1998)

High-resolution Brillouin spectroscopy was used to investigate the elastic properties of $[NH_3(CH_3)]_5Bi_2Cl_{11}$. The temperature dependences of nine phonon modes propagating in the directions [100], [010], [001], [110], [101], and [011] were obtained in the temperature range from 120 to 330 K. Strong correlations were found with the electric polarization mode which exhibits anomalous behavior at 307 and 170 K. A theoretical explanation of the experimental observations was given in terms of Landau-type free energy expansion for two inequivalent sublattices. Discussion was provided regarding the possible types of couplings between strain tensor components and spontaneous polarization.
[S0163-1829(98)07345-7]

I. INTRODUCTION

$[NH_3(CH_3)]_5Bi_2Cl_{11}$ (MAPCB) belongs to the family of alkyammonium halogenoantimonate (III) and bismuthate (III) crystals showing an interesting sequence of phase transitions.[1] At 307 K, MAPCB undergoes a ferroelectric continuous phase transition from the prototype phase *mmm* (space group *Pcab*) to the ferroelectric $mm2$ phase (space group $Pca2_1$). This transition has been extensively studied using a few different methods.[2–8] The dielectric dispersion[2] and Raman-scattering studies[3] indicate the order-disorder mechanism of this phase transformation. Another phase transition manifested by a nonlinear increase of spontaneous polarization at about 170 K was detected in pyroelectric measurements[1] and thermal properties studies.[4] The appearance of an excess polarization was accompanied by a nonlinear decrease of dielectric permittivity and an excess peak in the specific heat with a shape different from the changes observed at 307 K. Temperature dependences of the dielectric constants ε_{33}, spontaneous polarization P_s, and specific heat C_p of MAPCB are schematically drawn in Fig. 1.

The mechanism of the phase transitions in MAPCB was suggested on the basis of structural studies of the motion of methylammonium cations.[9,10] In the high-temperature phase (*mmm*) two cations are ordered while the other three are disordered. The observed disorder consists of two equilibrium positions for each site between which the cation can jump. In the ferroelectric phase one methylammonium cation becomes ordered whereas the remaining two are still disordered. In Ref. 10 Lefebvre, Carpentier, and Jakubas discussed the evolution of the probability for the two-site position model to describe the contribution of different types of cations to spontaneous polarization just below $T_c = 307$ K and around an inflection point at $T^* \approx 170$ K. Moreover, these authors suggest the existence of a monoclinic phase below 250 K. This suggestion is based on the results of a fit

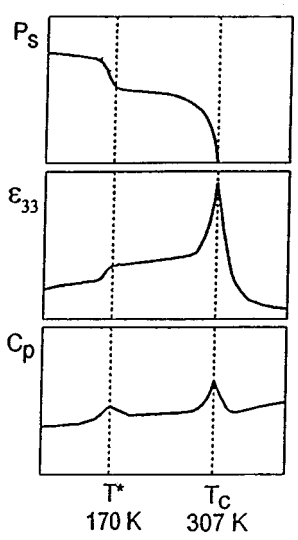

FIG. 1. Schematic diagram of temperature changes of spontaneous polarization, dielectric constant and specific heat of MAPCB crystals.

of their structural data to the space group $P2_1$. The obtained results indicate a spontaneous increase of the monoclinicity angle below 250 K. However, the temperature dependence of the cell parameters does not show the critical behavior at this temperature range. The postulated phase diagram[10] allows the existence of the ferroelastic phase below 250 K.

Ferroelectrics which undergo an order-disorder phase transition show a steplike change of the sound velocity in the vicinity of T_c. If additionally there exists an acoustic mode which is piezoelectrically coupled to polarization fluctuations, the Brillouin experiment can provide some dynamical dielectric information at frequencies in the range 10–15 GHz.

Elastic properties of MAPCB crystals have been studied using the ultrasonic technique in the temperature range 280–340 K covering only the main ferroelectric phase transition at 307 K. All sound velocities, measured in the principal crystallographic directions, showed critical slowing down at $T_c = 307$ K.[11] It was found that the anomalous parts of Δv_{22} and Δv_{33} are proportional to $\ln(T - T_c)$ in the high-temperature phase. Such changes could indicate that both dipole-dipole interactions and the short-range potential contribute to the ferroelastic phase transition in MAPCB.

In a recent paper Mielcarek *et al.*[12] reported results of piezoelectric studies of MAPCB crystals. The piezoelectric properties of this material measured in the kHz frequency range were found to be highly correlated with spontaneous polarization. Piezoelectric moduli d_{31}, d_{32}, and d_{33} were found to be strongly temperature dependent, especially around $T^* = 170$ K. The reverse elastic compliance coefficients $(S_{11})^{-1}$, $(S_{22})^{-1}$, and $(S_{33})^{-1}$ were also found to be strongly temperature dependent while no elastic softening was detected.

The suggestion regarding the possible ferroelastic nature of this material requires experimental verification as the monoclinic symmetry of the crystal observed below 250 K is a necessary condition for the ferroelastic phase transformation. The sufficient conditions for this transformation are (1) the presence of an elastic domain structure observable in polarized light and switchable by external mechanical stress, (2) spontaneous deformation of the crystal lattice or spontaneous onset of the angle of monoclinicity upon the postulated transformation of the $mm2Fm$ type, and (3) the presence of a soft acoustic phonon manifested as the disappearance of one of the diagonal transverse elastic constants (in the case considered this would involve c_{66}).

At present, no satisfactory theoretical model exists which would comprehensively describe changes in the physical properties of the material studied. Strukov *et al.*[4] proposed a Landau free energy expansion to the eighth power with respect to spontaneous polarization P_s in order to determine basic thermodynamic parameters, in particular the temperature changes in the specific heat C_p. In view of the above, the studies presented in this paper were undertaken to (a) determine elastic properties of the MAPCB crystal in a broad range of temperatures including its phase transitions at 307 and 170 K, (b) verify the hypothesis regarding the presence of the ferroelastic phase of this material below 250 K, and (c) propose a consistent theoretical model to explain the temperature changes of the order parameter and their effect on the crystal's elastic properties, and temperature dependencies of entropy and specific heat. We believe we have accomplished the above objectives.

II. EXPERIMENTAL PROCEDURE

Single crystals of MAPCB were grown[12] in the reaction of $(BiO)_2CO_3$ with CH_3NH_3Cl in concentrated HCl. The synthesized compound was purified by repeated crystallizations. Colorless and transparent crystals were obtained in the form of orthorhombic prisms. The temperature dependence of MAPCB crystal density was found from the x-ray studies ($\rho = 2.28$ g/cm^3 at 300 K). Samples with four different orientations were prepared to study the Brillouin scattering from the phonon modes propagating in six directions: [100], [010], [001], [110], [101], and [011]. The typical size of the samples was $3 \times 3 \times 4$ mm^3.

The Brillouin spectrometer has been described in detail elsewhere.[13] The incident light, polarized perpendicularly to the scattering plane, was provided by a stabilized single-mode argon-ion laser (Coherent series 2020) operating at 514.5 nm. The scattered light was analyzed at 90° with the use of a piezoelectrically scanned triple-pass Fabry-Perot interferometer (Burleigh RC-110) with the free spectral ranges of 16.12, 18.27, and 22.40 GHz. The spectra were accumulated with a photon-counting data acquisition and stabilization system (DAS-1, Burleigh).

Sound velocities v were deduced from the measured frequency shifts $\Delta\nu$ using the Brillouin equation

$$v = \lambda \Delta \nu (n_i^2 + n_s^2 - 2 n_i n_s \cos \Theta)^{-1/2}, \tag{2.1}$$

where λ is the wavelength of the incident light, n_i and n_s are the refractive indices for the incident and scattered light, respectively, and Θ is the scattering angle ($\Theta = 90°$). The values of the refractive indices of MAPCB were taken from Ref. 14. The Brillouin-scattering experiments were performed in the temperature range from 130 to 340 K using the cryostat described in a previous paper.[15] The temperature of the sample was controlled with a stability of ± 0.03 K.

III. EXPERIMENTAL RESULTS

The elastic stiffness tensor of both paraelectric and ferroelectric phase point groups mmm and $mm2$ contains nine dependent components (c_{11}, c_{22}, c_{33}, c_{44}, c_{55}, c_{66}, c_{12}, c_{13}, and c_{23}). The sound velocities v of the three acoustic waves propagating in the direction Q can be determined from the solution of the equation of motion which is given be the vanishing of the secular determinant[16]

$$|c_{ijkl} q_j q_k - \rho v^2 \delta_{il}| = 0, \tag{3.1}$$

where c_{ijkl} are elastic stiffness tensor components, q_j, q_k direction cosines of Q, and ρ is the density of the crystal. Following Ref. 22, Table I presents expressions of ρv^2 as a function of the elastic constants for the orthorhombic system for different geometries. Nine of the twelve modes listed in Table I have been observed in our experiment. It was evident from the obtained plots of $\Delta\nu(T)$ that each of the observed modes was affected by the ferroelectric transition at 307 K. Based on the behavior of the γ_1 mode, apart from T_c two additional characteristic temperatures can be distinguished, namely, 200 and 170 K. At about 200 K a sudden increase of

TABLE I. ρv^2 as a function of the elastic constants of orthorhombic MAPCB following Ref. 22.

Phonon	modes		elastic constants or their combinations
[100]	γ_1	L	[a] c_{11}
	γ_2	T_1	c_{66}
	γ_3	T_1	c_{55}
[010]	γ_4	L	[a] c_{22}
	γ_5	T_1	c_{44}
	γ_6	T_1	c_{66}
[001]	γ_7	L	[a] c_{33}
	γ_8	T_1	c_{55}
	γ_9	T_1	c_{44}
[110]	γ_{10}	QL	[a] $\frac{1}{4}\{c_{11}+c_{22}+2c_{66}+[(c_{22}-c_{11})^2+4(c_{12}+c_{66})^2]^{1/2}\}$
	γ_{11}	QT_1	[a] $\frac{1}{4}\{c_{11}+c_{22}+2c_{66}-[(c_{22}-c_{11})^2+4(c_{12}+c_{66})^2]^{1/2}\}$
	γ_{12}	QT_2	$\frac{1}{2}(c_{44}+c_{55})$
[110]	γ_{13}	QL	[a] $\frac{1}{4}\{c_{22}+c_{33}+2c_{44}+[(c_{33}-c_{22})^2+4(c_{23}+c_{44})^2]^{1/2}\}$
	γ_{14}	QT_1	[a] $\frac{1}{4}\{c_{22}+c_{33}+2c_{44}-[(c_{33}-c_{22})^2+4(c_{23}+c_{44})^2]^{1/2}\}$
	γ_{15}	QT_2	$\frac{1}{2}(c_{55}+c_{66})$
[101]	γ_{16}	QL	[a] $\frac{1}{4}\{c_{11}+c_{33}+2c_{55}+[(c_{33}-c_{11})^2+4(c_{13}+c_{55})^2]^{1/2}\}$
	γ_{17}	QT_1	[a] $\frac{1}{4}\{c_{11}+c_{33}+2c_{55}-[(c_{33}-c_{11})^2+4(c_{13}+c_{55})^2]^{1/2}\}$
	γ_{18}	QT_2	$\frac{1}{2}(c_{44}+c_{66})$

[a]Indicates which modes have been observed in the present experiment.

the Brillouin frequency shift was observed. Then $\Delta\nu$ remained constant and at 170 K started to grow with a distinctly higher slope. Similar changes were observed for the quasitransverse modes γ_{11} and γ_{14} propagating in the [110] and [011] directions. Such behavior indicates strong interactions of the elastic waves with the order parameter in a wide temperature range covering T_c at 307 K and T^* at about 170 K.

The results obtained for $\Delta\nu(T)$ allowed us to calculate the temperature dependences of all the elastic stiffness components of MAPCB (see Fig. 2). The influence of the ferroelectric phase transition on the elastic constants c_{11}, c_{22}, and c_{33} is similar to that observed using the ultrasonic technique.[11] We have observed a change in the slope of $c_{11}(T)$ at T_c and a steplike change of $c_{33}(T)$. The only difference has been found for the c_{22} elastic constant. From the ultrasonic studies it appears that c_{22} shows a decrease at 307 K and then goes gradually down with a lowering temperature. We found from the Brillouin experiment that a small dip of c_{22} takes place at T_c with an anomalous lowering below the room temperature. At about 280 K, the temperature behavior of c_{22} becomes ''normal'' and its value increases on cooling the sample. In order to illustrate the elastic dispersion of MAPCB crystal, in Fig. 2(a) we present the temperature dependences of reverse elastic compliances S_{ij}^{-1} as calculated from the piezoelectric data presented in Ref. 12. It is evident that the highest elastic anisotropy was found along the z axis [please examine $(c_{ij}-S_{ij}^{-1})$ in different directions for comparison]. Such changes indicate soft lattice properties in the spontaneous polarization direction and are in agreement with the mechanism of the ferroelectric phase transition as proposed in the structural investigations of Refs. 9 and 10.

In order to describe the temperature changes of the remaining elastic constants of MAPCB let us first examine simple tensorial relations between the strain components and spontaneous polarization P_s. The ferroelectric phase transition $mmm \rightarrow mm2$ is related to the vanishing of the mirror plane m at 307 K. This causes the onset of spontaneous polarization P_3 along the z axis and, of course, the crystal becomes piezoelectrically active. For the ferroelectric point group $mm2_z$ the piezoelectric tensor d_{ijk} contains five nonzero components, namely, d_{311}, d_{322}, d_{333}, d_{113}, and d_{223}. Combining two equations: the first one describing the piezoelectric effect $P_i = d_{ijk}S_{jk}$ with Hooke's law $\sigma_{jk} = c_{jklm}\epsilon_{lm}$, one can easily find those elastic constants affected by the temperature changes of P_s. In our case $P_3 \neq 0$ and $P_1 = P_2 = 0$, so the coupling piezoelectric moduli are d_{311}, d_{322}, and d_{333}. Hence, only the diagonal components of the strain tensor ϵ_{11}, ϵ_{22}, and ϵ_{33} may be coupled to P_s via a linear term in P_s which limits the number of the linearly affected elastic constants to the following six: c_{11}, c_{22}, c_{33}, c_{12}, c_{13}, and c_{23}. However, a biquadratic coupling between strain tensor components and polarization may also be present as we discuss at the end of Sec. IV (see Table II). The latter effect appears to be responsible for the anomaly in the c_{44} temperature dependence.

Let us now examine the temperature dependences of those elastic constants of MAPCB not measured using the ultrasonic or piezoelectric method, namely, c_{44}, c_{55}, c_{66}, c_{12}, c_{13}, and c_{23}. For the pure transverse elastic constants the greatest anomaly was found for c_{44}. It shows a 4% steplike change from the value of 0.20×10^{10} at 330 K and then grows very fast to reach the value of 0.98×10^{10} Nm^{-2} at 130 K. The c_{55} elastic constant shows a change in slope at 307 K whereas c_{66} was found to be unaffected by the ferroelectric phase transition within the accuracy of our experiment. The strong temperature dependence of the c_{44} elastic constant is reflected in the temperature behavior of c_{23} which shows an anomalous peak at T_c. Similar temperature

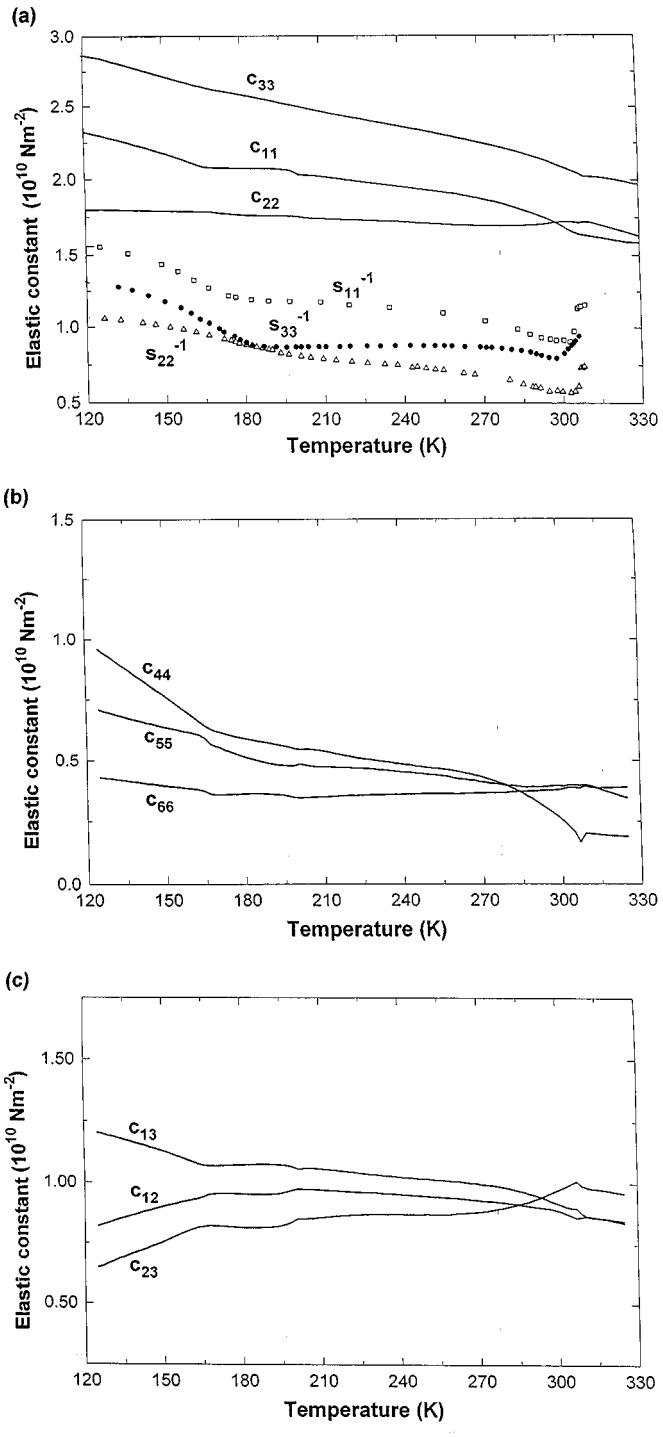

FIG. 2. Elastic constants of MAPCB versus temperature: (a) c_{11}, c_{22}, and c_{33} compared to the respective reverse elastic compliances S_{ij}^{-1} as found from piezoelectric measurements, (b) c_{44}, c_{55}, and c_{66}, and (c) c_{12}, c_{13}, and c_{23}.

changes have been reported for another ferroelectric compound, i.e., $(NH_4)_2ZnCl_4$.[17,18] The c_{12} and c_{13} elastic constants show small anomalies at T_c.

IV. THE THEORETICAL MODEL

We intend to develop a phenomenological Landau-based model in two stages. The first stage will be concerned only with electric polarization while the second one will be devoted to developing a coupling mechanism with elastic degrees of freedom.

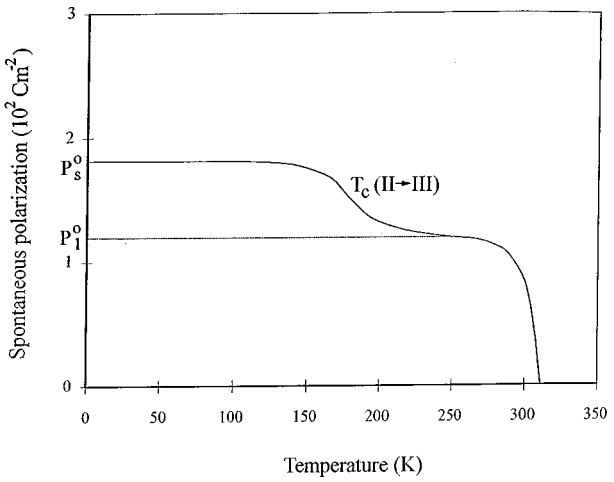

FIG. 3. Temperature dependence of spontaneous polarization of MAPCB, following Ref. 7.

A. Electric polarization

The theoretical analysis of the electric polarization will be based on the experimental plot of the total spontaneous polarization P_s as a function of temperature T. This is shown in Fig. 3, following Ref. 7. It is noteworthy that $(P_s^0-P_1^0)/P_1^0 = P_2^0/P_1^0 \approx \frac{1}{2}$ as can be clearly seen in Fig. 3 at $T=0$ K. Combining this with the information that the compound has two sublattices, it indicates that the plot $P_s(T)$ above reflects two distinct order-disorder transitions, each of which affects a single sublattice.

Following Ref. 9 we interpret the sequence of phase transitions exhibited in the temperature range studied as the gradual ordering of the methylammonium ($CH_3NH_3^+$) cations which possess a permanent dipole moment. Lefebvre, Carpentier, and Jakubas[9] argued that three of the five methylammonium cations are still disordered at 349 K while at 294 K only two of them are disordered. Hence the transition at 307 K involves the ordering of one sublattice and the one at 170 K another sublattice, both of which are composed of different sets of methylammonium ions. The plot of polarization in Fig. 3 strongly indicates that the dipole moment per site p_1^0 in the sublattice that orders at 307 K is twice as large as the one for the sublattice which orders at 170 K, p_2^0. We assume that the number of sites in each sublattice is the same, i.e., $N_1=N_2$ and hence $p_1^0=2p_2^0$.

The latter situation results in an effective ''spin'' variable $p_2^0=\frac{1}{2}$ for the second sublattice and $p_1^0=1$ for the first sublattice so that the ground state degeneracy in each sublattice is $g_i=2p_i^0+1$; $i=1,2$ and an equal occupation of the sublattices. The concept of an effective spin arsing from either one or two ordering dipole moments is shown in Fig. 4. For modelling purposes, we adopt this ansatz and carry out a requisite analysis which in the end, demonstrates a reassuring amount of consistency with experimental data as will be discussed later in the paper. However, the issue of the precise nature of the dipole sublattices requires further experimental determination.

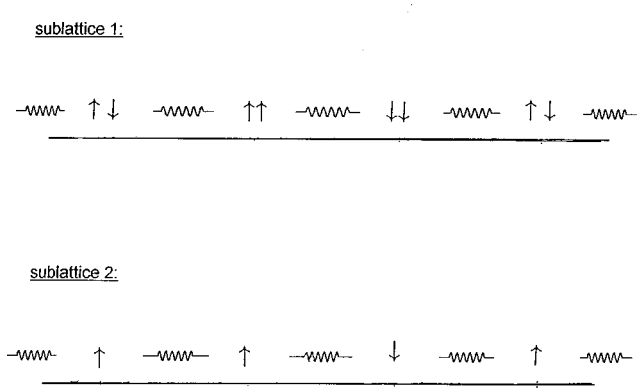

FIG. 4. Arrangements of ordering dipole moments at a given lattice site for each of the two sublattices of methylammomium.

Our starting point is a free energy expansion for the polarization degrees of freedom. We postulate that the two sublattices interact albeit weakly, and hence

$$F=F_1(P_1)+F_2(P_2)+F_{12}(P_1,P_2), \tag{4.1}$$

where the free energy per lattice site is given by

$$\frac{F_1(P_1)}{N_1}=\frac{A}{2}\,(T-T_1)p_1^2+\frac{B}{4}\,p_1^4-TS_1(p_1) \tag{4.2}$$

and applies to the first sublattice. Here, we have denoted $p_1=P_1/N_1$ and the maximum polarization per site $p_1^0=P_1^0/N_1$ is normalized to unity consistently with the assumption about two ions per site undergoing a simultaneous ordering transition, and T_1 is the expansion temperature close to 307 K. Similarly,

$$\frac{F_1(P_2)}{N_2}=\frac{a(T-T_2)}{2}\,p_2^2+\frac{b}{4}\,p_2^4-TS_2(p_2), \tag{4.3}$$

where T_2 is the second expansion temperature close to the transition temperature at 170 K and the maximum polarization per site in the second sublattice $p_2^0=P_2^0/N_2$ is normalized to $\frac{1}{2}$ consistently with the assumption about only one ion per site being ordered. Consequently, the entropy formulas for the effective spin variables p_1 and p_2 are (see Ref. 19 for rigorous derivation), for the effective spin-$\frac{1}{2}$ case,

$$\frac{S_2}{k_B}=\ln\left\{\sqrt{\frac{1+2p_2}{1-2p_2}}+\sqrt{\frac{1-2p_2}{1+2p_2}}\right\}-\left\{p_2\,\ln\left(\frac{1+2p_2}{1-2p_2}\right)\right\}, \tag{4.4}$$

where $|p_2|\leqslant\frac{1}{2}$ and, for spin 1,

$$\frac{S_1}{k_B}=\ln\left\{\frac{3p_1^2+(2-\sqrt{4-3p_1^2})^2}{p_1^2-(2-\sqrt{4-3p_1^2})^2}\right\}-\left\{p_1\ln\left(\frac{p_1+2-\sqrt{4-3p_1^2}}{p_1-2+\sqrt{4-3p_1^2}}\right)\right\}, \tag{4.5}$$

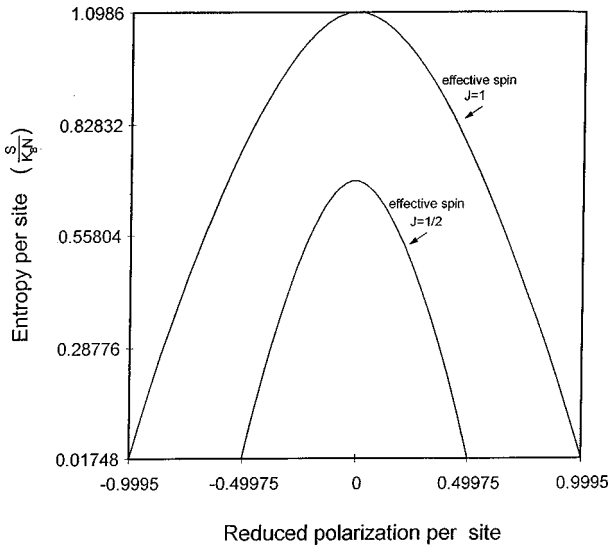

FIG. 5. Reduced entropy S/k_BN as a function of polarization per site for effective spins $\frac{1}{2}$ and 1.

where $|p_1|\leqslant 1$ and k_B is the Boltzmann constant. The plot of entropy as a function of polarization in both cases is shown in Fig. 5.

Finally, the coupling between the two sublattices has been chosen in the simplest possible form, i.e., as a bilinear term

$$F_{12}(P_1,P_2)=\frac{N}{2}\,\gamma p_1 p_2. \tag{4.6}$$

Note that $\gamma<0$ is required to obtain a correct effect of sublattice 1 on sublattice 2. Figure 6(a) shows what happens to the total polarization,

$$P=P_1+P_2=N_1p_1+N_2p_2, \tag{4.7}$$

as a function of temperature when $\gamma>0$, while Fig. 6(b) applies to the physically acceptable case of $\gamma<0$. The potential energy in each of the free energy components has been chosen to be in the Landau form, i.e.,

$$U(p)=\frac{A_2}{2}\,p^2+\frac{A_4}{4}\,p^4. \tag{4.8}$$

Here, $A_2=a(T-T_0)$, where $T_0=T_1$ or T_2 for $p=p_1$ or p_2, respectively, is the ''bare'' (i.e., with no sublattice coupling) critical temperature, or expansion temperature, of each sublattice treated separately (see Fig. 7). This yields classical critical exponents, in particular $\beta=\frac{1}{2}$. We have found $\beta\approx 0.518$ for our model parameters while the experiment gives $\beta=0.49\pm 0.03$, which is fairly consistent.

Subsequently, we carry out a free energy minimization procedure (assuming that $N_1=N_2=N/2$), i.e., solve the following two coupled algebraic equations:

$$0=\frac{\partial F}{\partial p_1}=A(T-T_1)p_1+Bp_1^3-T\,\frac{\partial S_1}{\partial p_1}+\gamma p_2 \tag{4.9}$$

and

$$0=\frac{\partial F}{\partial p_2}=a(T-T_2)p_2+bp_2^3-T\,\frac{\partial S_2}{\partial p_2}+\gamma p_1. \tag{4.10}$$

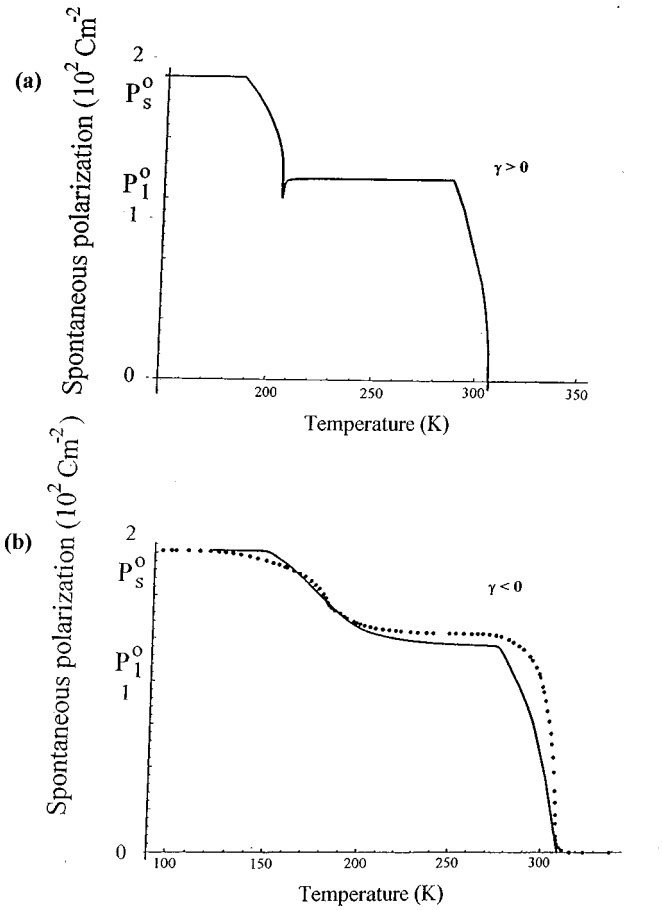

FIG. 6. The plot of total polarization P versus absolute temperature for (a) $\gamma>0$ and (b) $\gamma<0$. The values adopted here are $\gamma=0.1$ and $\gamma=-0.1$, respectively.

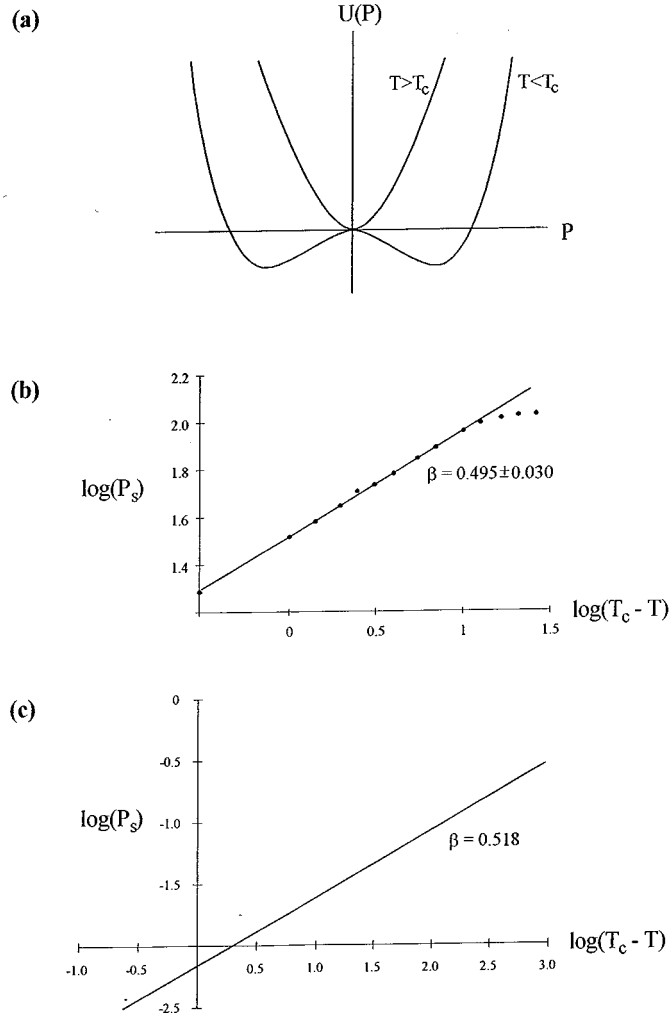

FIG. 7. Plots of (a) $U(P)$ versus T, (b) $\log P$ versus $\log(T-T_c)$—experiment, and (c) $\log P$ versus $\log(T-T_c)$—theory.

The role of entropy is to provide a saturation value for each sublattice polarization. When $T \ll T_1$ but $T \simeq T_2$, the first sublattice acts as an external field on the second sublattice which is seen in Fig. 6(b) in the precursor tail of polarization leading to the second transition.

Furthermore, we have calculated the free energy F as a function of temperature [see Fig. 8(a)] and the entropy as a function of temperature $S(T)$ [see Fig. 8(b)] and finally the excess specific heat [Fig. 8(c)] which closely resembles experimental plots [Fig. 8(d), see Iwata *et al.*[20] and Strukov *et al.*[4]].

In order to make contact with earlier models we first note that close to the transition temperature (for small polarization values) the entropy can be expanded in a power series according to

$$\frac{S_i}{k_B} \cong \ln(2p_i^0+1) - \frac{9}{2p_i^0(p_i^0+1)}\, p_i^2 + \cdots , \qquad (4.11)$$

where $p_i^0=1$ or $\frac{1}{2}$ depending on the choice of the sublattice $i=1,2$, respectively. On the other hand, close to saturation we have

$$\frac{S_i}{k_B} \approx (p_i^0 - |p_i|)\ln(p_i^0 - |p_i|) \qquad (4.12)$$

which prevents polarization per site p_i from exceeding the maximum allowed value p_i^0, which would be unphysical. It can be concluded, therefore, that the entropy term plays a twofold role: (i) it gives the saturation value to the polarization variables $P_i^0 = N_i p_i^0$ $(i=1,2)$, (ii) it renormalizes the free energy expansion coefficients including the transition temperatures.

The latter statement will allow us to carry out an approximation procedure where Eqs. (4.9) and (4.10) are replaced by their third order polynomial estimates

$$0 = \tilde{A}(T-T_c)p_1 + Bp_1^3 + \gamma p_2 + \cdots \qquad (4.13)$$

and

$$0 = \tilde{a}(T-T^*)p_2 + bp_2^3 + \gamma p_1 + \cdots . \qquad (4.14)$$

Here, we have introduced dressed expansion coefficients

$$\tilde{A} = A + \frac{9}{2}k \quad \text{and} \quad \tilde{a} = a + 12k \qquad (4.15)$$

based on the approximation in Eq. (4.11). Simultaneously, the actual transition temperatures are expressed in terms of the Landau expansion temperatures T_1 and T_2 as

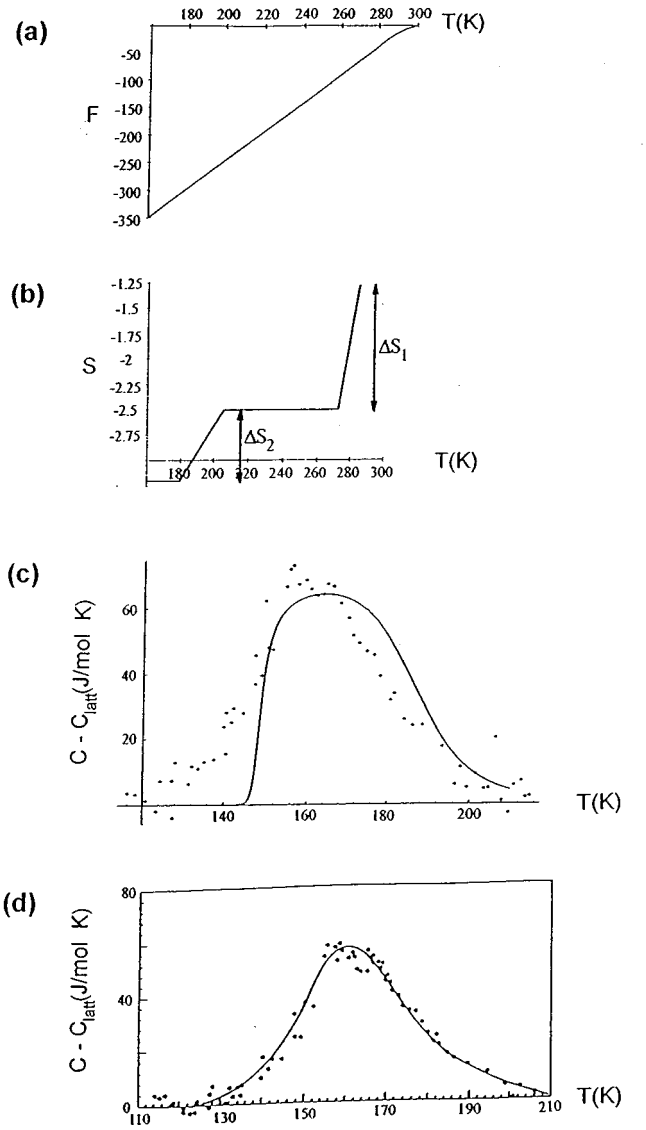

FIG. 8. Plots of (a) the scaled free energy (in arbitrary units) as a function of absolute temperature, (b) the entropy $S(T)$, and (c) the specific heat $C_p(T)$—theory as compared to the experimental plots (d).

$$T_c=\frac{A}{A+(9/2)k}\,T_1 \quad \text{and} \quad T^*=\frac{a}{a+12k}\,T_2. \tag{4.16}$$

Note first that for $T\leqslant T_c$, $p_2\approx 0$ and hence we end up with standard mean-field behavior for p_1, i.e.,

$$p_1(T)\cong\pm\sqrt{-\frac{\tilde{A}(T-T_c)}{B}} \tag{4.17}$$

with its attendant mean-field exponent of $\beta\approx 0.5$. For $T\leqslant T^*$, on the other hand, $p_1\cong p_1^0=\text{const}$ and the equation of state for p_2 is identical in form to the one for a prototype second order phase transition in the presence of an external field, namely,

$$\tilde{a}(T-T^*)p_2+bp_2^3\approx E, \tag{4.18}$$

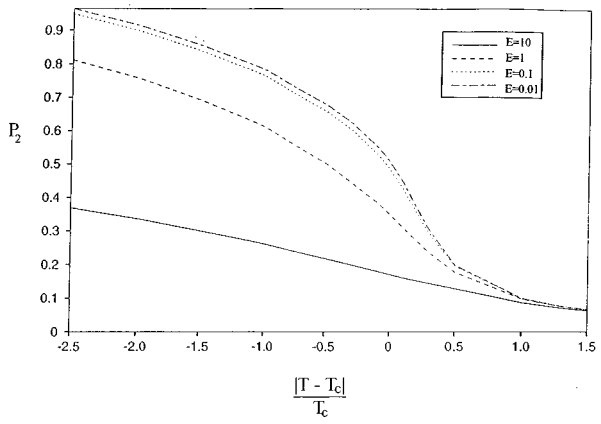

FIG. 9. A set of plots of polarization per site p_2 of the second sublattice normalized to unity, as a function of reduced temperature $(T-T_2)/T_2$ for a set of values of the effective field E given in the panel.

where $E\cong\gamma p_1^0$ is an effective field due to the first sublattice. This explains the characteristic long tail behavior of the second sublattice's polarization (see Fig. 9).

Finally, in the intermediate range of temperatures we must use a more accurate approach. We solve Eq. (4.13) for p_2 in terms of p_1 and substitute into Eq. (4.14) or alternatively into the free energy formula to obtain an effective (up to the eighth order) expansion:

$$F_{\text{eff}}=A_{\text{eff}}p_1^2+B_{\text{eff}}p_1^4+C_{\text{eff}}p_1^6+D_{\text{eff}}p_1^8, \tag{4.19}$$

where one finds the renormalized coefficients in terms of model parameters as

$$A_{\text{eff}}=-\frac{\tilde{A}}{2}\,(T-T_c)+\frac{a(T-T^*)\tilde{A}^2(T-T_c)^2}{2\gamma}, \tag{4.20}$$

$$B_{\text{eff}}=-\frac{3}{4}\,B+\frac{a(T-T^*)\tilde{A}^2(T-T_c)B}{\gamma^2}+\frac{b}{4}\,\frac{\tilde{A}^4(T-T_c)^4}{\gamma^4}, \tag{4.21}$$

$$C_{\text{eff}}=\frac{a(T-T^*)B^2}{2\gamma^2}+\frac{b\tilde{A}^3(T-T_c)^3B}{\gamma^4}, \tag{4.22}$$

$$D_{\text{eff}}=-\frac{3}{2}+\frac{b\tilde{A}^2(T-T_c)^2B}{\gamma^3}. \tag{4.23}$$

Note that Iwata *et al.*[20] gave a similar expansion in their Eq. (1) and stated that (in our notation)

$$A_{\text{eff}}=a(T-T_c),\quad B_{\text{eff}}>0,\quad C_{\text{eff}}<0,\quad D_{\text{eff}}>0. \tag{4.24}$$

Furthermore Strukov *et al.*[4] listed numerical values of three of these parameters, i.e.,

$$2A_{\text{eff}}/(T-T_c)=8.3\times 10^7 Vm/C, \tag{4.25}$$

$$4B_{\text{eff}}=3.4\times 10^{12} Vm^5/C^3, \tag{4.26}$$

and

TABLE II. A summary of the experimental results for the elastic coefficients and theoretical modelling. (+) and (−) refer to the sign of the coupling term used in the model free energy.

	Elastic constants of MAPCB around characteristic temperatures		
Type of coupling term used	p_2 around 170 K	p_2 around 200 K	p_1 around 307 K
$\epsilon^2 P(+)$[a]	c_{55}, c_{66}	c_{11}, c_{22}, c_{13}	c_{11}
$\epsilon^2 P(-)$		c_{12}, c_{23}	
$\epsilon P(+)$			c_{22}, c_{33}, c_{12}
$\epsilon P(-)$			c_{23}, c_{13}
$\epsilon^2 P^2(+)$	c_{11}, c_{33}, c_{44}		
$\epsilon^2 P^2(-)$	c_{12}, c_{23}		

[a]Applies to the changes presented in Fig. 10.

$$6C_{\text{eff}} = 3.3 \times 10^{15} Vm^9/C^5. \tag{4.27}$$

We are therefore, in qualitative agreement with earlier theoretical models attempting to explain the effect under consideration.

B. Elastic degrees of freedom

We now come to the issue of how polarization couples with elastic degrees of freedom. Based on Rehwald's review paper,[21] we can distinguish three general types of coupling terms between polarization P and elastic strain ϵ as follows.

Case (a). The lowest order contribution to the free energy is $\Delta F = \beta P \epsilon$, leading to a change of the elastic coefficient given by

$$\Delta c = \beta^2/2\alpha(T_c - T) \quad \text{for} \quad T < T_c \tag{4.28}$$

and

$$\Delta c = \beta^2/\alpha(T - T_c) \quad \text{for} \quad T > T_c. \tag{4.29}$$

In our case, evidence for this type of coupling can be seen in the temperature dependences of the elastic coefficients c_{22}, c_{33}, c_{12}, c_{23}, and c_{13} around 307 K and it involves p_1 in this interaction.

Case (b). The lowest order contribution to the free energy is $\Delta F = \gamma P^2 \epsilon$, leading to a discontinuous jump in the elastic coefficient

$$\Delta c = \gamma^2/2a_4. \tag{4.30}$$

This type of coupling does not seem to be present in the case studied in this paper.

Case (c). The lowest order contribution to the free energy is $\Delta F = \delta P \epsilon^2$ which results in a change of the elastic coefficient proportional to the order parameter's mean value $\langle P \rangle$, i.e.,

$$\Delta c = 2\delta \langle P \rangle. \tag{4.31}$$

This type of coupling appears to involve p_2 and affect c_{55} and c_{66} around 170 K, c_{12}, c_{23}, c_{11}, c_{22}, and c_{13} around 200 K and, finally c_{11} around 307 K via the involvement of p_1.

In analyzing our experimental situation we must account separately for coupling to both sublattices and, consequently,

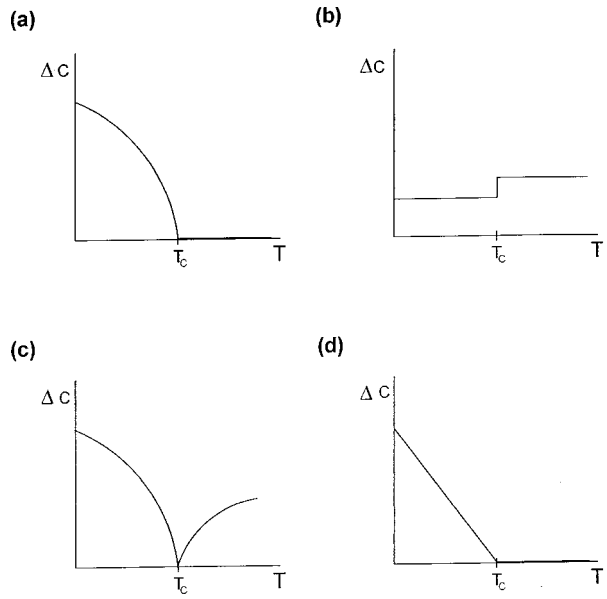

FIG. 10. Schematic plots of the increments of the elastic coefficients (in arbitrary units) Δc due to four different types of coupling between polarization and strain components (a) $\Delta F = \beta P \epsilon$, (b) $\Delta F = \gamma P^2 \epsilon$, (c) $\Delta F = \delta P \epsilon^2$, and (d) $\Delta F = \mu \epsilon^2 P^2$.

to two critical regimes: (a) close to 307 K and (b) close to 170 K. A summary of our measurements of the elastic coefficients with the postulated forms of ΔF is given in Table II. Note that in addition to the standard coupling terms: $P\epsilon$, $P\epsilon^2$, and ϵP^2 we have also included the biquadratic coupling case (d) where the lowest order contributions to the free energy is chosen as $\Delta F = \epsilon^2 P^2$ in order to account for the vicinity of $T^* \cong 170$ K and, in particular, for the anomalous behavior of c_{44} but also c_{11}, c_{33}, c_{44}, c_{12}, and c_{23} to some degree. The shapes of Δc in the three cases (a)–(c) discussed by Rehwald[21] as well as case (d) mentioned above are shown in Fig. 10. Clearly, if $P \cong P_0(T - T_c)^{\beta}$, then in the case (d) of Fig. 10 we postulate $\Delta c = 2\mu P_0^2 (T - T_c)^{2\beta}$ for $T \leqslant T_c$, and with $\beta = \frac{1}{2}$ we obtain the required linear relationship with T. Once again good qualitative agreement between experiment and theoretical modeling is found.

V. CONCLUSIONS

The results presented above lead to the following conclusions. The data regarding the elastic properties of MAPCB crystals, obtained by the Brillouin-scattering method, indicate their strong correlation with the order parameter P_s in a wide temperature range, including the region around and below $T^* = 170$ K. No softening of acoustic phonons was observed in the vicinity of 250 K where the existence of a ferroelastic phase was postulated. The proposed theoretical description based on the assumption about the existence of two sublattices with different values of the effective dielectric polarization ''spin variables'' ($p_2^0 = \frac{1}{2}$ and $p_1^0 = 1$, respectively) provides an internally consistent and a qualitatively correct model explaining changes in the polarization, as well as thermal and elastic properties of the material studied. The agreement of our experimental data with the proposed theoretical description allows one to assume that over a broad temperature range the polarization of the first sublattice acts

as an effective external field $E=\gamma N_1 p_1^0$ for the second sublattice. Admittedly, this is at present only a simplifying theoretical hypothesis and it requires experimental verification before it can be endorsed without qualifications.

There are still some unanswered questions, especially with respect to the nature of the piezoelectric coupling terms as shown in Table II. Clearly, the form of c_{11} at T_c does not agree with the symmetry of the crystal which is centrosymmetric above T_c. The remaining coupling terms appear to agree with symmetry requirements but we must keep in mind that at T^* the transition exhibited does not introduce a symmetry change.

ACKNOWLEDGMENTS

This research was supported by grants from NSERC (Canada) awarded to H.K., M.J.C., and J.A.T. One of the authors (B.M.) wishes to thank the Spanish Ministry of Education and Culture for supporting him with a sabbatical grant (No. SAB95-0460).

[1] R. Jakubas and L. Sobczyk, Phase Transit. **20**, 163 (1990).
[2] C. Pawlaczyk, R. Jakubas, K. Planeta, Ch. Bruch, J. Stephan, and H.-G. Unruch, Ferroelectrics **126**, 145 (1992).
[3] P. Carpentier, J. Lefebvre, and R. Jakubas, J. Phys.: Condens. Matter **4**, 2985 (1992).
[4] B. A. Strukov, R. Poprawski, S. A. Taraskin, and J. Mróz, Phys. Status Solidi A **143**, K9 (1994).
[5] M. Iwata and Y. Ishibashi, J. Phys. Soc. Jpn. **59**, 4239 (1990).
[6] M. Iwata and Y. Ishibashi, J. Phys. Soc. Jpn. **61**, 4615 (1992).
[7] J. Mróz and R. Jakubas, Ferroelectrics **118**, 29 (1991).
[8] J. Mróz and R. Jakubas, Ferroelectr. Lett. Sect. **11**, 53 (1990).
[9] J. Lefebvre, P. Carpentier, and R. Jakubas, Acta Crystallogr., Sect. B: Struct. Sci. **47**, 228 (1991).
[10] J. Lefebvre, P. Carpentier, and R. Jakubas, Acta Crystallogr., Sect. B: Struct. Sci. **51**, 167 (1995).
[11] R. Jakubas, J. Lefebvre, H. Fontaine, and P. Fracois, Solid State Commun. **81**, 515 (1992).
[12] S. Mielcarek, P. Biskupski, Z. Tylczyński, B. Mróz, and R. Jakubas, Phys. Status Solidi A **158**, 427 (1996).
[13] B. Mróz, H. Kiefte, M. J. Clouter, and J. A. Tuszyński, Phys. Rev. B **46**, 8717 (1992).
[14] A. Miniewicz and R. Jakubas, J. Mol. Struct. **5**, 55 (1991).
[15] B. Mróz, H. Kiefte, M. J. Clouter, and J. A. Tuszyński, Phys. Rev. B **36**, 3745 (1987).
[16] L. D. Landau and E. M. Lifshitz, *Theory of Elasticity* (Addison-Wesley, New York, 1959).
[17] C. A. Smolensky, I. G. Siny, S. D. Prokhorowa, E. G. Kuzminov, and R. Lauho, Ferroelectrics **36**, 351 (1981).
[18] A. M. Gillet, Y. Luspin, and G. Hauret, Solid State Commun. **64**, 797 (1987).
[19] J. A. Tuszyński and W. Wierzbicki, Am. J. Phys. **59**, 555 (1991).
[20] M. Iwata, T. Tojo, T. Atake, and Y. Ishibashi, J. Phys. Soc. Jpn. **63**, 3751 (1994).
[21] W. Rehwald, Adv. Phys. **22**, 721 (1973).
[22] R. Vacher and L. Boyer, Phys. Rev. B **6**, 639 (1972).